THE

PHYSICAL REVIEW

Many-Body Approach to the Atomic Hyperfine Problem.
I. Lithium-Atom Ground State*†

Edward S. Chang, ‡ Robert T. Pu, and T. P. Das

Department of Physics, University of California, Riverside, California

(Received 9 October 1967)

The Brueckner-Goldstone many-body perturbation method, previously utilized
for calculations of atomic correlation energies and polarizabilities, has been extended to
the study of the hyperfine structure. The correlation energy as well as the hyperfine coupling
constant of the lithium atom are calculated and compared with the results of some earlier
methods. The present method makes use of Feynman-like diagrams which facilitate the
evaluation of the importance of various physical effects. Analysis of the hyperfine diagrams
shows that the difference between the experimental and the Hartree-Fock values is mainly
accounted for by spin polarization, although correlation effects are by no means negligible.
Our result of 2.887 a.u. agrees very well with the experimental value of 2.9096 a.u. The
excellent result for the total energy of −7.478 a.u., comparing with the corresponding
experimental value of −7.47807 a.u., shows that the wave function is good over-all, as well
as in the region near the nucleus.

I. INTRODUCTION

Theoretical investigations on the properties of
atoms are usually based on the Hartree-Fock ap-
proximation in which each electron is assumed to
move independently in the average potential of oth-
er electrons. In this approximation, the Pauli
principle is satisfied by choosing for the many-
electron wave function a determinantal form built
out of one-electron states characterized by quan-
tum numbers n, l, s, m_l, and m_s. In the restrict-
ed Hartree-Fock approximation (RHF), the addi-
tional assumption is made that the spatial part of
one-electron orbitals is independent of m_s — the so-
called spin equivalence restriction. The RHF pro-
cedure usually leads to energies within 1% of ex-
periment. The difference is called correlation en-
ergy, and is associated with the instantaneous cor-
relation between the electrons as opposed to the
averaged correlation included in the Hartree-Fock
approximation. The RHF approximation is also
too restrictive in another aspect — it does not per-
mit the core electrons to make any contribution to
the magnetic hyperfine interaction.

In order to allow the core electrons to contribute
to the spin density at the nucleus, one uses the un-
restricted Hartree-Fock approximation[1,2] (UHF),
where the spin equivalence restriction is removed.
However, the UHF approximation leads to other
problems in that the many-electron wave function
is no longer an eigenfunction of S^2, a result that
contradicts a well-known consequence of the com-
mutation properties of the nonrelativistic Hamil-
tonian. Secondly, an uncertain amount of correla-
tion is inadvertently included[3] in the UHF theory.

The first difficulty may be resolved by restoring
the UHF function to be an eigenfunction of S^2, by pro-
jecting out the desired spin component. In this re-
gard it is an important question whether the projec-
tion is done following or preceding the minimiza-
tion of energy. The former procedure, labeled
UHFP, has led to worse results for the hyperfine
constant of lithium atom than UHF.[4] It has been
pointed out by Marshall that it is physically more
reasonable to minimize the energy after projec-
tion.[5] Such a procedure, labeled PUHF, leads to
a hyperfine result in closer agreement with exper-
iment. However, the PUHF approximation of ne-
cessity requires the use of multideterminantal
wave functions, which introduce severe computa-
tional difficulties. In addition, this multidetermi-
nantal nature of the PUHF function also leads to an
uncertain amount of correlation.[3]

Several attempts have been made to understand
the role of correlation effects in influencing wave
functions and energies of atoms. Most of the meth-
ods that have been employed can be classified
broadly into two categories. One, the Hylleraas-

type procedure,[6,7] involves the explicit use of inter-electronic coordinates in the atomic wave function and the other, commonly called a configuration interaction procedure,[8] uses a variational function involving a linear combination of determinantal functions, each representing a particular configuration of the electrons in the atom. Both procedures suffer from certain common difficulties. First, there is the question of the most suitable form of the trial function for the best convergence. Since there are no general ground rules for the best choice of variational functions, there is a certain element of chance involved in carrying out these procedures successfully for any particular atom. Second, both methods are computationally rather difficult to extend to heavier atoms, because one has too many interelectronic coordinates or too many configurations to take into account. Third, physical interpretation in both procedures is made difficult because the wave function is no longer explicitly one-electron–like in nature.

The Brueckner-Goldstone many-body theory has recently been applied to the problem of correlation energies and polarizabilities of atomic systems.[9] This procedure has been developed in the spirit of perturbation theory, using the Hartree-Fock function as the zeroth order. Using the second quantization formalism, one can associate Feynman-like diagrams with various orders of perturbation analogous to quantum electrodynamics. As with any perturbational method, the important criterion here is the convergence in terms of orders of perturbation. It has been shown[9] that for the correlation energy the convergence of the perturbation series is good, and one obtains accurate results from just a few lowest orders. The perturbational nature of the Brueckner-Goldstone (BG) method has additional advantage in terms of numerical accuracy, since one now handles small quantities of the order of the difference between the actual and Hartree-Fock Hamiltonians directly rather than the difference of large numbers. For instance, one calculates the correlation energy directly in BG theory rather than as the small difference of the total and Hartree-Fock energies which are individually large. Perhaps the greatest advantage of the BG procedure is that it provides a good conceptual picture of the nature of correlation effects. In particular, one can partition the correlation diagrams into classes, one of which represents purely intrashell correlations, another pure intershell correlation, and, finally, one which is a mixture of both.

In this paper the BG method is extended to the calculation of the atomic hyperfine coupling constant (hfs). This property is interesting as a sensitive test of the goodness of the atomic wave function near the nucleus, in contrast to the energy which is an averaged property. When combined with polarizability and scattering studies[10] which depend on the peripheral region of the atom, it allows for a detailed mapping of the atomic wave function in all regions. The BG method also allows for separate calculation of contributions to the hfs from different physical effects such as correlation and spin polarization, and so one can obtain a fair assessment of their relative importance. In this method,

the wave function is an eigenfunction of S^2 to each order of perturbation; one can therefore examine the effects of departure from an eigenfunction of S^2 by an analysis of the pertinent diagrams. Furthermore, the analysis of various diagrams and their contributions can provide answers regarding the nature of the approximations in RHF, UHF, PUHF, and other methods. Finally, as in the case of correlation energy, one can make formal spin cancellations in diagrams prior to numerical evaluations, in common with the exchange perturbation[11] and the moment perturbation methods.[12] Thus one again deals directly with small numbers instead of taking the difference of large hfs associated with each core spin state as in the UHF procedure.

While the techniques employed in this paper are applicable to any general atom, we have specialized to the case of the lithium ground state for two main reasons. First, it is the simplest representative example of an open-shell atom. Its study provides an understanding of the interplay between correlation and exchange effects in terms of their influence on the hfs. Secondly, the lithium atom is of interest in its own right, since it is the most extensively investigated atom as regards both correlation energy and hfs. Several papers on lithium have dealt with the influence of correlation and exchange effects on hfs by different procedures. The situation regarding the origin of the hfs is still not completely understood. Some of the papers indicate that correlation and spin polarization effects are nearly independent and can be dealt with separately.[3,5] Other investigations tend to show that correlation effects alone can adequately explain the experimental hfs without invoking the concept of spin polarization.[13] The BG approach is particularly suitable for the examination of this question, because certain diagrams can be associated with correlation effects, while others pertain to spin polarization effects.

In Sec. II the BG theory will be briefly reviewed with special emphasis on its application to the calculation of the hfs and the correlation energy. Detailed consideration will be made of the potential and the wave function specifically for the lithium atom. Section III will deal with the evaluation of the hfs. In Sec. IV the correlation energy will be calculated and the implications of the results for both properties in terms of their bearing on the theory, and comparison with experiment will be discussed. In Sec. V we will present a few concluding remarks about the merits and shortcomings of the BG method and its applicability to other systems.

II. THE BRUECKNER-GOLDSTONE THEORY. APPLICATION TO LITHIUM ATOM

A. Resumé of the BG Theory

In atomic units ($e = \hbar = m_e = a_0 = 1$), the nonrelativistic Hamiltonian for a system of N electrons and a heavy nucleus of charge Z, in the absence of external fields, is

$$H = \sum_{i=1}^{N} T_i + \sum_{i=1}^{N} \sum_{j>i}^{N} v_{ij} \tag{1}$$

where

$$T_i = -\tfrac{1}{2}\nabla_i{}^2 - Z/r_i \quad \text{and} \quad v_{ij} = 1/|\vec{r}_i - \vec{r}_j|. \tag{2}$$

Let the true ground-state wave function of the atom be designated by Ψ_0, satisfying the Schrödinger equation

$$H\Psi_0 = E\Psi_0. \tag{3}$$

The Brueckner-Goldstone theory involves a perturbation approach in which the zeroth-order approximation has the two-body potentials v_{ij} replaced by effective one-body potentials V_i. The difference between the exact and approximated potentials is treated as the perturbation. That is

$$H = H_0 + H' , \tag{4}$$

$$H_0 = \sum_{i=1}^{N} T_i + \sum_{i=1}^{N} V_i , \tag{5}$$

and

$$H' = \sum_{i=1}^{N} \sum_{j>i}^{N} v_{ij} - \sum_{i=1}^{N} V_i. \tag{6}$$

The single-particle potential V is chosen to be Hermitian, and it generates a complete orthonormal set of single-particle orbitals ϕ_n satisfying

$$(T + V)\phi_n = \epsilon_n \phi_n. \tag{7}$$

The BG perturbation theory utilizes the second-quantization formalism, with these single-particle orbitals as the basis states. In this case, Eqs. (5) and (6) are replaced by

$$H_0 = \sum_n \epsilon_n \eta_n{}^\dagger \eta_n \tag{8}$$

and

$$H' = \sum_{p,q,m,n} \tfrac{1}{2}\langle pq|v|mn\rangle \eta_p{}^\dagger \eta_q{}^\dagger \eta_n \eta_m$$
$$- \sum_{p,q} \langle p|V|q\rangle \eta_p{}^\dagger \eta_q. \tag{9}$$

The "unperturbed" ground state of the atom satisfies

$$H_0 \Phi_0 = E_0 \Phi_0, \tag{10}$$

and is a determinant formed from the N single-particle orbitals lowest in energy. The single-particle states are called unexcited if they are contained in Φ_0 and excited if they are not. An occupied excited state is called a particle, and an unoccupied unexcited state a hole. The $\eta^\dagger$ and η operators in Eqs. (8) and (9) obey the usual Fermi-Dirac anticommutation relations. They have the following physical meaning: $\eta_m{}^\dagger$ is a particle creation operator if m is an excited state, but a hole destruction operator if m is an unexcited state; on the other hand, η_m is a hole creation operator or a particle destruction operator.

In the BG perturbation theory, the exact ground state of the atom is given by:

$$\Psi_0 = \sum_{n=0}^{\infty}{}^L \left(\frac{1}{E_0 - H_0}H'\right)^n \Phi_0, \tag{11}$$

where L means that only linked diagrams are to be included. The total energy E in Eq. (3) can be expressed as

$$E = E_0 + \Delta E,$$

where $\Delta E = \langle \Phi_0|H'|\Psi_0\rangle.$ $\tag{12}$

It is convenient to use a diagrammatic representation of the perturbation expansion (11) in analogy with problems in quantum electrodynamics. Then the unperturbed ground state of the atom, Φ_0, is considered the "vacuum" state, and is represented by no lines whatsoever. The perturbation interactions v and V are represented by ---• and ---×. Particles and holes are drawn as solid lines directed, respectively, upward and downward. The "time axis" is considered as directed upward, so that a diagram for Ψ_0 never has any free lines at the bottom. These diagrams carry an algebraic sign defined by $(-1)^{h+l+n_V}$ where h is the number of internal hole lines, l the number of closed loops, and n_V the number of V interactions. Goldstone defines the unlinked part of a diagram as any part without external lines, which is completely disconnected from the rest. A diagram with no unlinked part is called linked.[14]

The convenient rules for drawing diagrams are summarized below:

1. Draw n horizontal interaction lines (dashed), where n corresponds to the order of the perturbation.

2. Each vertex is traversed by two (solid) lines, where one is always directed towards and the other away from it.

3. Discard all unlinked diagrams.

4. Make sure that the number of external hole lines equals the number of external particle lines.

5. In labeling graphs, include only all distinct combinations, but ignore the exclusion principle.

B. Expectation Value of an Operator

In practice Ψ_0 cannot be calculated to all orders, and must be truncated at a particular order of perturbation. The expectation value of a Hermitian operator Op is then given by

$$\langle \text{Op} \rangle = \frac{\langle \Psi_0|\text{Op}|\Psi_0\rangle}{\langle \Psi_0|\Psi_0\rangle}. \tag{13}$$

Since all higher orders of Ψ_0 are orthogonal to the unperturbed or zeroth-order function Φ_0, which is normalized, the normalization integral is given by

$$\langle \Psi_0|\Psi_0\rangle = 1 + \langle \Psi_0^{(1)}|\Psi_0^{(1)}\rangle + \langle \Psi_0^{(1)}|\Psi_0^{(2)}\rangle$$
$$+ \langle \Psi_0^{(2)}|\Psi_0^{(1)}\rangle + \cdots, \tag{14}$$

where $\Psi_0^{(0)} = \Phi_0$, $\Psi_0^{(1)}$, $\Psi_0^{(2)}$, $\cdots \Psi_0^{(n)}$, represent various orders of perturbation in the wave function as given by (11). Similarly the numerator of (13) can also be expanded in various orders,

$$\langle \Psi_0|\text{Op}|\Psi_0\rangle = \langle \Psi_0^{(0)}|\text{Op}|\Psi_0^{(0)}\rangle$$
$$+ 2\langle \Psi_0^{(0)}|\text{Op}|\Psi_0^{(1)}\rangle + \cdots$$
$$+ \langle \Psi_0^{(m)}|\text{Op}|\Psi_0^{(n)}\rangle + \cdots,$$

where each term is composed of a number of diagrams. All diagrams belonging to $\langle \Psi_0^{(m)}|\text{Op}|\Psi_0^{(n)}\rangle$ are referred to as (m,n) diagrams.
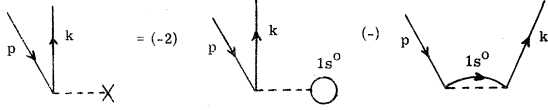
FIG. 1. Diagrammatic definition of V^{N-1} for Li. p is an unexcited state and k an excited state.

When Op is the total Hamiltonian, there is an alternative procedure because of Eq. (3). On multiplying this equation on the left by Φ_0^* and integrating over all coordinates, one obtains

$$E = \langle \Phi_0 | H | \Psi_0 \rangle, \tag{15}$$

which is equivalent to (12), since

$$\langle \Phi_0 | H | \Psi_0 \rangle = E \langle \Phi_0 | \Psi_0 \rangle = E.$$

C. Choice of the Single-Particle Potential V

In making use of the BG perturbation theory, it is first necessary to obtain a complete set of single-particle states determined by the potential V in Eq. (7). The choice of V is not unique. However, convergence considerations indicate the desirability that the basis states generated with this potential resemble closely the one-electron ground and excited states of the N-electron system. A particularly convenient choice designated as $V^N - 1$ will be utilized here.[9] Its definition, in terms of matrix elements, is

$$\langle i | V^{N-1} | j \rangle = \sum_{n=1}^{N-1} (\langle in | v | jn \rangle - \langle in | v | nj \rangle). \tag{16}$$

In the summation, the $(N-1)$ lowest HF orbitals are used. The potential V^{N-1} thus chosen generates a complete set of bound and continuum states which closely resemble the occupied and excited HF states of the system. In particular, the Nth occupied state of the complete set is identical to the highest occupied HF state. The difference between the actual and calculated lower occupied HF states does not lead to any serious difficulty because there are diagrams which correct these orbitals back to the HF orbitals.

A typical matrix element in (16) is given by

$$\langle in | v | jn \rangle = \int d\vec{r}_1 \int d\vec{r}_2 \, \phi_i^*(\vec{r}_1) \phi_n^*(\vec{r}_2)$$

$$\times (1/r_{12}) \phi_j(\vec{r}_1) \phi_n(\vec{r}_2). \tag{17}$$

For the ground state of the lithium atom, the V^{N-1} potential is defined by

$$\langle i | V_{Li}^{N-1} | j \rangle = 2 \langle i 1s^0 | v | j 1s^0 \rangle - \langle i 1s^0 | v | 1s^0 j \rangle \tag{18}$$

for all angular momenta l. The $1s^0$ orbital used in (18) was taken from Roothaan, Sachs, and Weiss.[15] Equation (18) is represented diagrammatically in Fig. 1.

D. The Wave Functions

With the potential for the lithium atom thus chosen, the single-particle state $\phi_i(\vec{r})$ can be written as $R_{k,l}(r)/r Y_l^m(\theta,\phi) \chi_S(m_S)$, where R_{kl} is the radial function, Y_l^m the spherical harmonic, and χ_S the spin function. The radial function satisfies

$$\left[\frac{d^2}{dr^2} - \frac{l(l+1)}{r^2} + \frac{z}{r} - 4 \left(\frac{1}{r} \int_0^r R_{1s^0}^2(r') dr' \right. \right.$$

$$\left. + \int_r^\infty \frac{R_{1s^0}^2(r')}{r'} dr' \right) + 2\epsilon_{k,l} \left. \right] R_{k,l}(r)$$

$$+ \frac{2}{2l+1} \left[\frac{1}{r^{l+1}} \int_0^r R_{1s^0}(r') R_{k,l}(r') r'^l dr' \right.$$

$$\left. + r^l \int_r^\infty \frac{R_{1s^0}(r')}{r'^{l+1}} R_{k,l}(r') dr' \right] R_{1s^0}(r) = 0. \tag{19}$$

This is an integrodifferential equation, where for $\epsilon_{k,l} < 0$, it has the additional difficulty of being an eigenvalue equation. The technical details of solving this equation are given in the appendix. Briefly, for $\epsilon_{k,l} > 0$, it is solved by combining the noniterative[16] and Numerov's methods[17]; for $\epsilon_{k,l} < 0$, an iterative method based on a program by Cooley[18] was used. The basis states thus generated include the $1s$ orbital (different from $1s^0$), the $2s$ (identical with the HF $2s^0$), the ns, np, etc., and continuum states for all l and k.

The eigenvalues for the basis states calculated by us are compared with those of the self-consistent HF orbitals in Table I. The two energies are virtually identical for the highest occupied HF state $2s$; small differences in the fifth significant figure are due to differences in computational accuracy. The $1s$ energies, on the other hand, are significantly different as expected. The $2p$ energies are presented to show the closeness of our calculated and the actual HF excited states.

The bound state orbitals are square-integrable and are normalized to unity in the usual manner. The continuum states have to be "normalized" in a different way, and we have chosen them to have the usual asymptotic form for Coulombic functions (charge unity),

$$R_{k,l}(r) \xrightarrow[r \to \infty]{} \cos[kr + (1/k) \ln(2kr)$$

$$- (\pi/2)(l+1) - \sigma_{k,l}] \tag{20}$$

$\sigma_{k,l}$ being a phase factor. In our calculation of matrix elements involved in the diagrams, a cutoff radius $R_0 = 50a_0$ was used. We have found, in common with earlier work,[9] that for different choices of cutoff radius in this range, the final results for a diagram are the same even though individual matrix elements may show slight variations.

TABLE I. Eigenvalues of V^{N-1} compared with the Hartree-Fock values (in a.u.).

Orbitals	Our basis states	SCFHF[15]
$1s$	−2.793 03	−2.477 75[a]
$2s$	−0.196 31	−0.196 32
$2p$	−0.128 66	−0.128 67[b]

[a]This value is taken from Clementi, because the Roothaan-Sachs-Weiss value is believed erroneous.

[b]D. A. Goodings, Ph.D. thesis, Cambridge University, England, 1961 (unpublished).

The zero-order wave function Φ_0 of Eq. (10) is taken to be a determinant built out of the lowest three occupied states $1s^+$, $1s^-$, and $2s^+$. The higher-order wave functions are obtained from (11) using various values of n. The evaluation of these higher-order functions from (11) requires the introduction of the complete set of states just calculated and having $\mathcal{K}_0$ in the denominator operate on them. Thus for the first-order function we have

$$\Psi_0^{(1)} = \sum_{j,k=1}^{\infty}{}' \sum_{m,n=1}^{N} \frac{|jk\rangle\langle jk|v|mn\rangle}{\epsilon_n + \epsilon_m - \epsilon_j - \epsilon_k}$$

$$- \sum_{k=N+1}^{\infty} \sum_{m=1}^{N} \frac{|k\rangle\langle k|V|m\rangle}{\epsilon_m - \epsilon_k}. \qquad (21)$$

The prime in the first summation signifies that at least one of j and k should be an excited state ($N+1 \to \infty$). This procedure involves summations over the quantum numbers l, m_l, and m_S. The discrete states require, in addition, a sum over their principal quantum numbers, while the continuum states involve an integration over k,

$$\sum_k \to (2/\pi)\int_0^{\infty} dk. \qquad (22)$$

The diagrams corresponding to the first-order wave function (21) are presented in Fig. 2. Using the definition (18) for V^{N-1}, Fig. 2(a) can be schematically expanded out in terms of the fictitious diagrams illustrated in Fig. 1. Since the $1s$ orbital differs only slightly from $1s^0$, Figs. 2(a), 2(b), and 2(c) very nearly cancel.

In the calculation of spin-dependent properties, there is further cancellation between spin-up and spin-down $1s^{\pm}$ states. The unpaired single-excitation diagram, Fig. 2(j), represents the spin-polar-
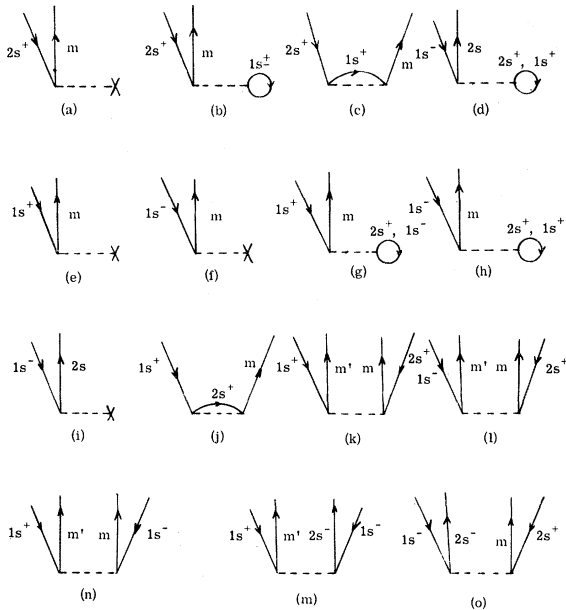
ization of the $1s$ core orbitals. It shows the virtual excitation of the $1s^+$ state to a higher s state through exchange interaction with the $2s^+$ state.

A single-excitation diagram can represent only one-body effects. Double-excitation diagrams, Figs. 2(k) through 2(o), describe two-body correlation effects, with 2(m) and 2(n) representing intershell effects and 2(k), 2(l), and 2(o) representing intrashell effects. As is well-known, the spin-polarized wave function by itself is not an eigenfunction of S^2. It will now be shown that the inclusion of Figs. 2(k) through 2(o) in the first-order wave function leads to an eigenfunction of S^2.

E. Eigenfunction of S^2

The zeroth-order wave function is, of course, an eigenfunction of S^2. It is well known that S^2 commutes with the total Hamiltonian H. Since V is spin-independent, H_0 and H' commute with S^2. Now the perturbed wave function Ψ_0 in (11) is a sum of terms of all orders, each order involving products of ratios $[1/(\epsilon_0 - H_0)]H'$ operating on Φ_0. Since $[H', S^2] = 0$ and Φ_0 is an eigenfunction of S^2, the perturbed wave function to each order is also an eigenfunction of S^2.

It is instructive to prove explicitly that the first-order wave function is indeed an eigenfunction of S^2. For this purpose one refers to the diagrams in Fig. 2. One only needs to group them in such a way that each group is an eigenfunction of S^2. Using a compact notation

$$\Phi_0 = \begin{pmatrix} 1s & 1s & 2s \\ \alpha & \beta & \alpha \end{pmatrix}, \qquad (23)$$

it can easily be seen that the following functions are also eigenfunctions of S^2 with the same set of quantum numbers L, M_L, S, and M_S:

$$A = \begin{pmatrix} m & m & n \\ \alpha & \beta & \alpha \end{pmatrix}, \qquad (24)$$

$$B = \begin{pmatrix} m & n & k \\ \alpha & \beta & \alpha \end{pmatrix} + \begin{pmatrix} n & m & k \\ \alpha & \beta & \alpha \end{pmatrix}. \qquad (25)$$

It is noted that with the ground state as described in (23), a spin-up excited state cannot be a $2s$ state whereas a spin-down excited state can. In the latter case one can have two diagrams, namely when the excited state is the $2s$ state and when it is not. This has been done in Fig. 2. The diagrams (a), (b), (c), (d), (i), and (m) can be seen to be of the form A in (24), while the others combine in pairs to give form B, namely [(e), (f)], [(g), (h)], [(k), (l)], [(j), (o)], and [(n), (n')], where (n') is the diagram obtained by a symmetric interchange of excited states m and m' in diagram (n). This completes the proof. The most significant pair of diagrams is [(j), (o)], representing a combination of single- and double-excitation diagrams. We interpret this as indicating that one has to admix some correlation to a spin-polarized wave function to obtain an eigenfunction of S^2.

III. THE HYPERFINE COUPLING CONSTANT

A. Experimental hfs

We shall first briefly review the experimental situation for the hfs in the ground state of the lithium atom. The only contribution to the splitting of
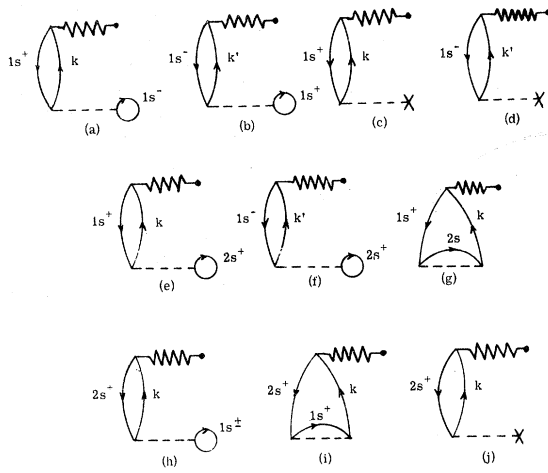

FIG. 2. First-order wave-function diagrams for Li. m and m' are excited states which do not include the $2s$ state.

FIG. 3. hfs diagrams classified as (0, 1). Here k stands for spin-up excited states and does not include $2s$. k' stands for spin-down excited states and includes $2s$.

the hyperfine levels comes from the Fermi contact term given in frequency units by[19]:

$$\Delta \nu = \frac{8}{3} \pi \frac{2I+1}{I} \mu_e \mu \langle f \rangle / 4\pi ,\qquad (26)$$

where $f = \sum_{i=1}^{N} \frac{2\delta(r_i)}{r_i^2} S_{z_i}$,

μ_e is the electronic magnetic moment which is 1.001 16 μ_B,[20] μ is the nuclear moment, and $\langle f \rangle$ is the spin density of the electrons at the nuclear site. $\Delta \nu$ has been measured accurately by molecular-beam magnetic-resonance methods to be 803.512 ± 0.015 Mc/sec.[21] The most recent value of the nuclear moment of Li^7 from molecular-beam measurements after applying diamagnetic corrections is $(3.256310 \pm 0.000085)\mu_N$.[22] The quantity $\langle f \rangle$ is sometimes loosely referred to as the hfs, and is evaluated from Eq. (24) to be 2.909 60 a.u. We will use this value as the experimental result[23] for comparison with theory.

B. Analysis of Diagrams

The hyperfine coupling constant can be calculated from Eq. (13), where the operator is now f. In general it is practicable to calculate Ψ_0 only to second order in the perturbation series. To this accuracy,

$$\text{hfs} = \frac{\langle 0+1+2 | f | 0+1+2 \rangle}{\langle 0+1+2 | 0+1+2 \rangle} \qquad (27)$$

where 0, 1, and 2 stand for the zeroth-, first-, and second-order wave functions, respectively. Using $\langle 0|0 \rangle = 1$ and $\langle 0|n \rangle = 0 (n \neq 0)$, Eq. (27) reduces to

$$\text{hfs} = (\langle 0|f|0 \rangle + 2\langle 0|f|1 \rangle + \langle 1|f|1 \rangle + 2\langle 0|f|2 \rangle$$
$$+ 2\langle 1|f|2 \rangle + \langle 2|f|2 \rangle)(1 + \langle 1|1 \rangle$$
$$+ 2\langle 1|2 \rangle + \langle 2|2 \rangle)^{-1} \qquad (28)$$

where $\langle n|f|m \rangle = \langle m|f|n \rangle$ because f is Hermitean.

The numerator of Eq. (28) can be expressed as a sum of diagrams, after introducing the symbol -⋀⋀⋀- for the Fermi contact operator. The diagrams are classified as (0, 0), (0, 1), (1, 1), (0, 2) and so on, for the first four terms.

Because of the orthogonality of the single-particle states, the expectation value of a sum of one-electron operators over determinantal wave functions is just the sum of expectation values of the operators over single-particle states. The (0, 0) hfs diagrams are composed of the sum of the spin densities of the $1s$ orbitals which exactly cancel, and the $2s$ orbital which gives 2.065. This result so far is identical to the ordinary RHF calculation using numerical procedures.

In the next order, the (0, 1) diagrams are drawn in Fig. 3. To make a proper distinction, k^+ is used to denote a spin-up excited state and k^- a spin-down excited state. Therefore, k^- includes $2s$ whereas k^+ does not. Because the spins in the diagrams are opposite, diagrams (a)–(f) cancel in pairs except whenever $k^- = 2s^-$. Even then, the residue diagrams $k^- = 2s$ in (b) and (d) almost cancel because of the definition of V. These cancellations represent the special merit of the diagrammatic technique which allows us to deal with small quantities directly rather than obtaining them as differences of larger ones. The diagrams (h), (i), and (j) also cancel except for the slight difference between $1s$ and $1s^0$. This difference would vanish if V^N had been used instead of V^{N-1} utilized in this work. Typically matrix elements involving the difference between $1s$ and $1s^0$ differ by only a few parts per thousand, and are ignored in all orders beyond (0, 1).

The only important diagram then is Fig. 3(g). It shows the $1s^+$ state interacting with the $2s^+$ state through the exchange potential and becoming an excited state which interacts with the hfs operator and then returns to the $1s^+$ state. Clearly this has the physical significance of being the spin-polarization mechanism. The rest of the diagrams in Fig. 3 give very small contributions as expected. The results from the diagrams of Fig. 3 are displayed in Table II. The results for $\sum_{k=9}^{\infty}$ bound are obtained as explained in the appendix.

TABLE II. Contributions to the hfs from (0, 1) diagrams (in a.u.). See Fig. 3.

Diagram	Contribution
(g) k = continuum	0.475 972
(g) $k = 3$–8	0.011 320
(g) $\sum_{k=9}^{\infty}$ bound[a]	0.000 926
(e) + (f) $k' = 2s$	0.028 350
(a) + (d) $k' = 2s$	−0.003 464
(h) − (j) k = continuum	−0.000 180
(h) − (j) k = bound	−0.000 180
Total	0.512 744

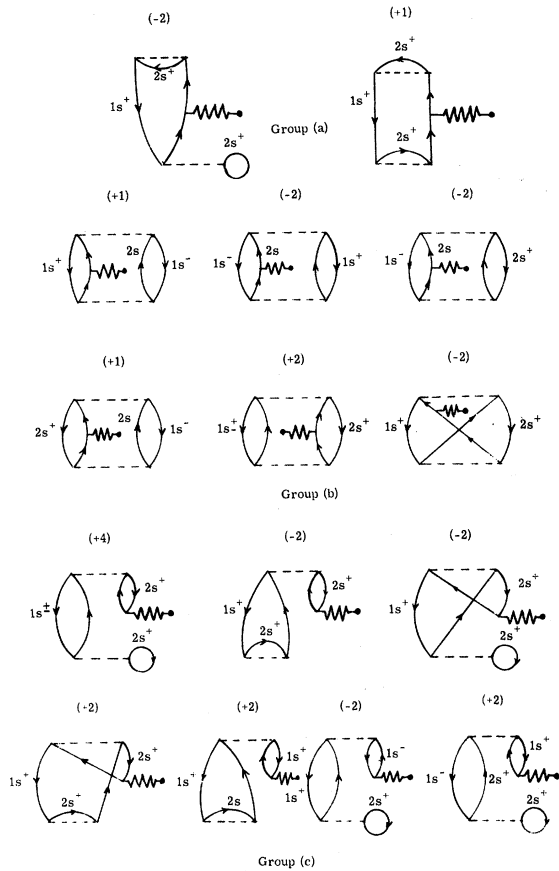[a]Estimated from the $n^{-3/2}$ rule, as explained in the appendix.

FIG. 4. hfs diagrams classified as (1,1). Group (a) consists of one-body diagrams, group (b) two-body, and group (c) hybridization of the two.

A conservative estimate of the accuracy of these numbers is about 5 parts per thousand. Small errors can arise from the numerical integration procedure and the fact that we integrate up to only k = 20 a.u. From Table II, the bound states are seen to contribute only 8% of the total spin polarization. This is in agreement with a previous calculation of Cohen, Goodings, and Heine,[11] where they expanded the exchange perturbed function in terms of bound Hartree-Fock states, and found only 10% of the expected spin-polarization effect. The preponderance of the contribution from the continuum states can be understood from the facts that both Coulomb and hfs matrix elements are larger for continuum than for bound excited states, and the continuum excited states span a larger volume of phase space than bound ones. Another useful observation is that in these diagrams involving just the first-order wave function, the particle state is always connected to a hfs vertex, and so only s states need to be included.

This last observation is particularly useful for the (1, 1) diagrams and makes their number tractable. They form three groups: (a) strictly one-particle, (b) strictly two-particle, and (c) diagrams involving both one and two particles. These

are shown in Fig. 4. Group (a) diagrams represent second-order effects of core polarization. Group (b) diagrams are associated with the effects of in-out correlation of both the intershell and intrashell types. Group (c) shows the interplay of core polarization and correlation effects. The (1, 1) diagrams add up to 0.020 a.u. and are composed of contributions −0.000 88, −0.000 805, and +0.021 150 from (a), (b), and (c).

The (0, 2) diagrams are of the same order in number of interactions (vertices) as the (1, 1) diagrams, but can only arise out of the second-order wave function. They can again be classified into three groups according to the number of particles. Figure 5 shows the strictly two-particle ones. The excited states j and k must have the same l, but l can have any value. This can be understood because the two-electron matrix elements all involve two unexcited s states, and would therefore vanish over angular integrations unless the two excited states had the same l. Figure 5 represents a specific many-body effect which can be visualized as follows. The intershell correlation produces an instantaneous polarization of the $1s^2$ core, which in turn attracts the $2s$ electron, increasing its spin density at the nuclear site. Diagram 5 is the corresponding effect of the exchange part of this potential. The contributions from continuum states only are displayed in Table III. From this table, it is seen that the contributions from excitations to d, f, and higher-l states are much smaller than from s and p. Between the latter two, the p-type contributions are somewhat larger, showing the dominance of dipole polarization. Contributions from diagrams involving bound excited states are expected to be relatively small from ex-
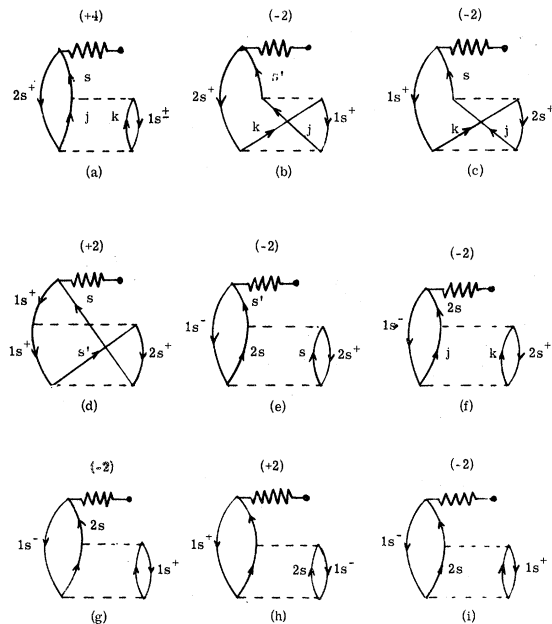

FIG. 5. hfs diagrams classified as (0, 2): two-particle type. s and s' stand for s states only, but j and k include all values of l.

TABLE III. Contributions to the hfs from certain (0,2) diagrams (in a.u.).

l/diagram	(a): direct	(b): exchange	(a) + (b)
0	+0.079 608	−0.038 386	+0.041 222
1	+0.059 344	−0.005 746	+0.053 598
2	+0.009 736	−0.000 354	+0.009 382
3	+0.002 540	−0.000 142	+0.002 398
Total	+0.151 228	−0.044 628	+0.106 600

Note: (a) + (b) including bound states (add 10%) = +0.117.

perience with the (0, 1) contribution. In fact, they were found to produce a 10% increase over the pure continuum results leading to a total of 0.117 from diagrams 5(a) and (b). Diagrams 5(c)–(f) represent the parallels of 5(a) and (b) in that they deal with the contributions to the hfs from the $1s$ states which have reacted to the polarization of the $2s$ orbital. Diagrams 5(c) and (d) nearly cancel each other in contribution. Diagrams 5(e) and (f) are really residual ones after account has been taken of spin-cancellation. They also make negligible contributions relative to 5(a) and (b) since they involve bound excited states. Together, diagrams 5(c) to (f) lead to only about 1% of the effect of 5(a) and (b).
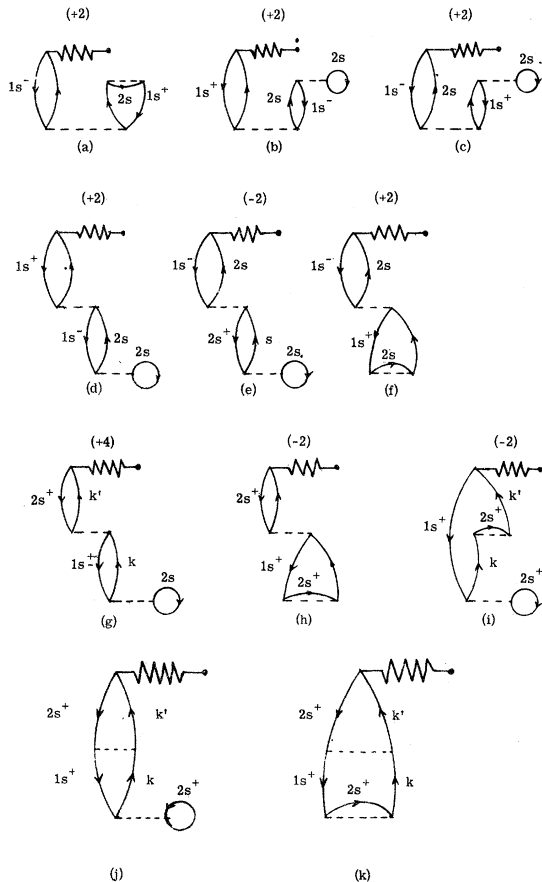

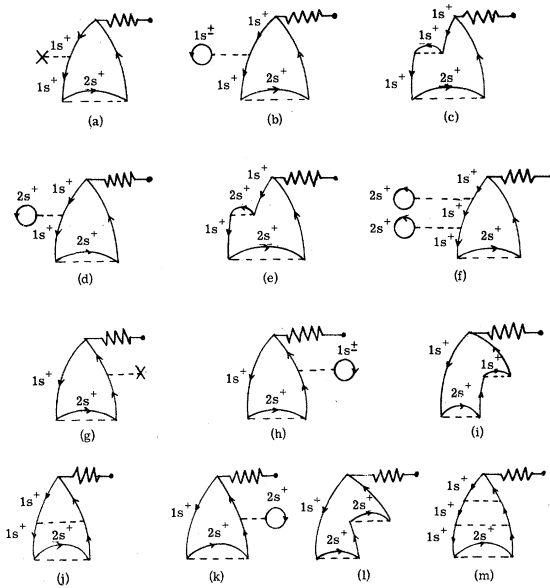FIG. 6. hfs diagrams classified as (0,2): hybridization and single-particle.

FIG. 7. EPV diagrams contributing to the hfs.

The mutual polarization of the $1s$ orbitals is shown in Figs. 5(g), (h), and (i); here again only the residues after spin-cancellations are displayed. These diagrams again involve at least one bound excited state and lead to negligible contribution compared to 5(a) and (b).

In the second group the hybridization of spin polarization and correlation results in the diagrams in Fig. 6(a), (b), and (c). The third group consists of various single-particle diagrams: Fig. 6(d)–(k). In all the diagrams [6(a)–(i)], only excited s states contribute. Diagrams 6(a)–(c) add up to 0.013 while 6(d)–(k) add up to only −0.0028.

In Sec. II, it was remarked that the $1s$ orbital obtained from the V^{N-1} potential would be somewhat different from the HF $1s^0$ orbital, but would be automatically corrected by the perturbation expansion. This "correction" can be seen to arise naturally from the perturbation series. Thus, in all diagrams considered, the hole or the particle could interact with a passive unexcited state in the next order of perturbation leading to hole-hole (h-h), or hole-particle (h-p) ladder diagrams. Kelly termed these exclusion-principle-violating (EPV) diagrams.

The results of this ladder effect on the core polarization diagram are shown in Fig. 7. Diagrams 7(a), (b), and (c) cancel because of the definition of V^{N-1}. The diagrams (d) and (e) can be summed to all orders following Kelly's technique of shifted energy denominator as follows. The unmodified diagram Fig. 3(g) differs from 7(d), and 7(d) in turn from 7(f) by the factor $x = \langle 1s\,2s \,|v\,|\,1s\,2s \rangle / (\epsilon_{1s} - \epsilon_k)$. Using the expansion,

$$1/(1-x) = 1 + x + x^2 + \cdots, \tag{29}$$

the combined effect of the ladder made up of d, f and higher orders and the corresponding exchange ladder involving e, etc., is to replace the denominator $(\epsilon_{1s} - \epsilon_k)$ of the unmodified diagram 3(g) by

$(\epsilon_{1s}-\epsilon_k + \langle 1s2s \,|\, v \,|\, 1s2s\rangle - \langle 1s2s \,|\, v \,|\, 2s1s\rangle)$. The interpretation of this result is that the $1s$ state in the V^{N-1} potential does not "see" the $2s$ state, as does the RHF $1s^0$. With the above modification, the $1s$ state now effectively sees the $2s$ electron so that ϵ_{1s} is changed to ϵ_{1s^0} within one part per thousand. This changes the core polarizatization contribution from 0.511 to 0.545 a.u., and it is the latter that should be compared with the results from EP and MP methods.

The diagrams 7(g)–(m) are $(h\text{-}p)$ diagrams. Diagrams (g), (h), and (i) cancel as before. Diagram (j) allows for the fact that the particle state excited from the $1s$ now no longer sees two $1s$ states, but only one. Diagrams (k) and (l) are analogous to (d) and (e), only here it is the particle and not the hole that interacts with the $2s$ state. Adding another "rung" to (j) gives (m). Interestingly, after integrating over the continuum states, the ratio of (m) to (j), and (j) to the unmodified diagram is again practically a constant (within 2%). An approximation similar to the $(h\text{-}h)$ diagrams where it was exact could then be made to sum these diagrams to all orders. Bound states in the unmodified diagram only contribute 0.05 a.u., and so ladder modifications to them can be ignored. The modified core polarization result is finally 0.675 a.u.

Laddering also affects $(1, 1)$ and $(0, 2)$ diagrams, but since their original contributions are already quite small, the modifications are negligible. Higher-order diagrams of the type $(1, 2)$, $(2, 2)$, and $(0, 3)$ are expected to be small, both because each order of interaction brings in a matrix element divided by an energy denominator, a factor lying between 0.01 and 0.1, and also since there is a large amount of cancellation. To verify this point, two of these higher-order diagrams [Figs. 8(a) and (b)] were evaluated. The contribution of Fig. 8(a) was calculated to be +0.001961 using continuum excited s states. Figure 8(b) is a three-body diagram, and was estimated to be less than +0.001. Since Fig. 8(b) appears to be the largest three-body hfs diagram, three-body effects on the hfs of the lithium atom appear to be negligible.

C. Normalization

Before summarizing the contributions of the various classes of diagrams, it is appropriate to discuss the normalization constant in the denominator of (28). The contributions to the normalization constant can also be handled by diagrammatic techniques. The lowest-order nontrivial normalization diagrams are classified as $(1, 1)$ and are given in
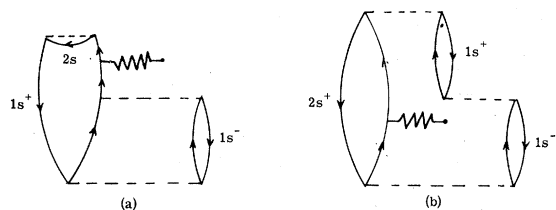

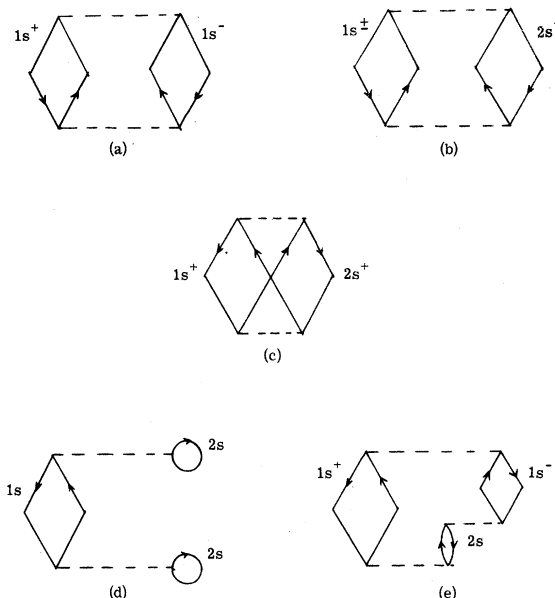FIG. 8. Higher-order hfs diagrams not included in the final result.

FIG. 9. Normalization diagrams. The particle and hole lines are bent to convey the additional denominators which distinguish these from energy diagrams.

Fig. 9. For example, the algebraic expression of diagram 8(a) is

$$\sum_{k}\sum_{k'}\left(\frac{\langle 1s\,1s\,|\,v\,|\,kk'\rangle}{\epsilon_{1s}+\epsilon_{1s}-\epsilon_k-\epsilon_{k'}}\right)^2 \tag{30}$$

The results from diagrams 9(a), (b), and (c) add up to 0.0028. One-body diagrams such as 9(d) and higher-order diagrams such as 9(e) are estimated to be 0.00001 and hence negligible. The net effect of normalization on the hfs calculation according to Eq. (28) is then to divide all the contributions already calculated by 1.0028.

D. hfs Results

To summarize the hfs results, the contributions from various diagrams are listed in Table IV. It appeared from these results that the hfs for the lithium atom arises from three main sources:

TABLE IV. Analysis of contributions to the hfs.

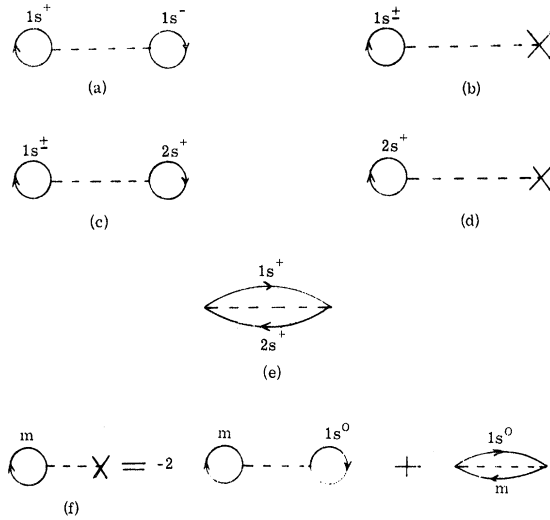| Diagrams	Description	Contribution (a.u.)
$(0, 0)$	$2s$ intrinsic	2.065
Fig. 3 + Fig. 7	core polarization all orders	0.685
Fig. 5	correlation	0.117
Fig. 4	S^2 considerations	0.020
Fig. 6(a), (b), and (c)	hybridization	0.013
Fig. 6(d)–6(k)	others	−0.003
Total		2.897
Total, including normalization effect		2.89 ± 0.02

FIG. 10. First-order energy diagrams. The diagrammatic equation (f) is the equivalent of the equation in Fig. (1). m stands for $1s^{\pm}$ or $2s^{\pm}$.

the intrinsic contribution of the $2s$ orbital, spin polarization, and intershell correlation. The intrinsic contribution is necessarily the same as from the RHF method. Spin-polarization contributes about 80% of the difference between the experimental and the RHF values, in excellent agreement with 78% obtained by Marshall using a PUHF procedure.[5] The intershell correlation effect contributes another 15%. The $(1,1)$ diagrams in Fig. 4 which restore the eigenfunction of $\vec{S}^2$ contribute about 2%, while diagrams combining one-particle and two-particle effects, referred to as hybridization, contribute another 1%. We have examined the contributions from several higher-order diagrams and found them insignificant. The neglect of the higher-order diagrams and possible errors in estimating diagrams which make very small contributions leads us to a conservative estimate of overall errors as 0.02 a.u. On including the normalization factor, our total calculated hfs comes out at 2.89 ± 0.02 as compared to the experimental value of 2.909 60 a.u. A comparison with results of other calculations and the over-all implications of our results will be discussed in Sec. V.

IV. ENERGY OF THE LITHIUM ATOM

A. Experimental Energy

Before discussing the calculation of the energy, we would like to comment on the experimental total energy for the lithium atom. The determination of the experimental energy is more indirect and therefore less precise than the hfs. Usually the total energy is estimated from successive ionization potentials, which are difficult to measure accurately. Fortunately, for the lithium atom one can obtain a reasonably precise value of the energy as follows. Pekeris has carried out an accurate variational calculation of the Li^+ ion using 1078 determinants.[24] His energy for the Li^+ ion is

considered to be accurate to one per billion from a comparison of his theoretical helium-atom energy with experiment. To obtain the energy of the Li atom one has to add to the energy of the Li^+ ion the first ionization potential ($2s$) of the lithium atom. From this sum one has to subtract off a relativistic correction to the $2s$ energy to obtain the total nonrelativistic energy of the atom, which is what we will calculate. Using an estimate of 0.000 001 8 a.u. for this relativistic effect, Scherr, Silverman, and Matsen[25] obtained for the nonrelativistic "experimental" energy of the lithium atom, $E_{exp} = -7.478\,07 \pm 0.0001$ a.u. (1 a.u. = 27.206 eV).

B. Calculation of Energy Diagrams-Correlation Energy

The prescription for calculating the energy has been given in (15). On expanding in orders of perturbation, for convenience,

$$E = E_0 + \sum_n{}^L \langle \Phi_0 | H'\{[1/(E_0 - H_0)]H'\}^n \, \Phi_0 \rangle. \quad (31)$$

It must be emphasized that the restriction "linked" for energy diagrams differs from the one for wavefunction diagrams. A linked energy diagram is constructed from corresponding linked wave-function diagrams by closing the free lines with $H' \, \Phi_0\rangle$.

The order of an energy diagram can be defined as the number of interaction lines in the diagram. The zeroth-order E_0 is just the sum of the one-electron energies.

$$E_0 = \epsilon_{1s} + \epsilon_{1s} + \epsilon_{2s}. \quad (32)$$

The first order is obtained from Eq. (31) with $n = 0$, and the diagrams are given in Fig. 10. As mentioned in Sec. II we have made use of the V^{N-1} single-particle potential. As indicated in Fig. 10, this potential can be expanded in terms of two-particle matrix elements, which leads to some cancellation of the first-order energy diagrams.

Had we chosen the V^N potential, as in the conventional Hartree-Fock approximation, the first-order diagrams remaining after cancellation would represent the usual subtraction of the Coulomb and exchange interactions between electrons which were counted twice in Eq. (32) for E_0. Hence

$$E_{HF}(V^N) = E_0^{HF} + E_1^{HF} = -7.432\,73 \text{ a.u.} \quad (33)$$

with the V^{N-1} potential

$$E_{HF}(V^{N-1}) = E_0 + E_1 = -7.432\,23 \text{ a.u.}, \quad (34)$$

which is very slightly (0.0005 a.u.) higher than $E_{HF}(V^N)$. Since the experimental energy is −7.478 05 a.u., the conventional correlation energy from $E_{HF}(V^N)$ is −0.045 32 a.u. With our choice of V^{N-1} potential, the corresponding "correlation" energy that one should obtain from the perturbation series is −0.045 82 a.u.

The second-order energy diagrams divide naturally into two groups: one-particle, Fig. 11(a), (b) and (c); and two-particle, Fig. 11(d), (e), and (f). The former would vanish for the V^N potential. In the present treatment, they sum up to −0.000 097 1 a.u., a negligible contribution to the correlation energy.
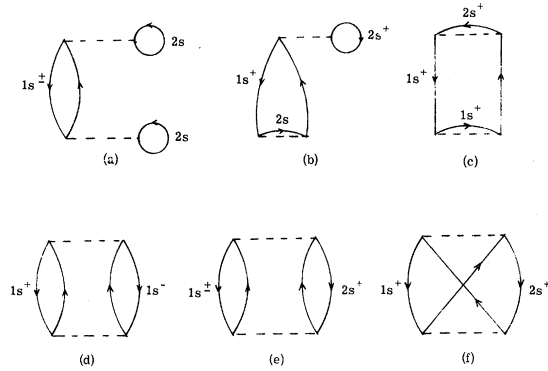
FIG. 11. Second-order energy diagrams. (a), (b), and (c) are one-body diagrams, and (d), (e), and (f) two-body.

Before analyzing the diagrams [11(d), (e), and (f)], it is convenient to decompose v in partial waves

$$v = \sum_l v_l = \sum_l \frac{r_<^l}{r_>^{l+1}} P_l(\cos\theta). \tag{35}$$

With this expansion, diagrams 11(d) and (e) lead to second-order energy terms

$$E_2^0(l;p,q) = \sum_k \sum_{k'} \frac{\langle pq|v_l|kk'\rangle\langle kk'|v|pq\rangle}{\epsilon_p + \epsilon_q - \epsilon_k - \epsilon_{k'}}, \tag{36}$$

where p and q are the particular unexcited states. The exchange diagram 11(f) has k and k' interchanged in the second matrix element in (36). These diagrams represent the main bulk of the correlation energy. The contributions from various orbital angular momenta and pairs of states are displayed in Table V.

From Table V one notices that the second-order energy accounts for more than 90% of the correlation energy indicating that the first-order wave function is quite adequate for this purpose. Furthermore, as in the case of hfs, the convergence in l is very rapid, the s and p excited states being the most important.

TABLE V. Second-order energy contributions[a] (the main part of the correlation energy).

l	$1s^+-1s^-$	$1s^--2s^+$	$1s^+-2s^+$
0	−0.013 446	−0.000 456	−0.000 077
1	−0.021 595	−0.001 032	−0.000 687
2	−0.003 426	−0.000 124	−0.000 042
3	−0.000 946	−0.000 030	−0.000 006
$\sum_{l=0}^{3}$	−0.039 413	−0.001 642	−0.000 812
Total	−0.041 867 a.u.		

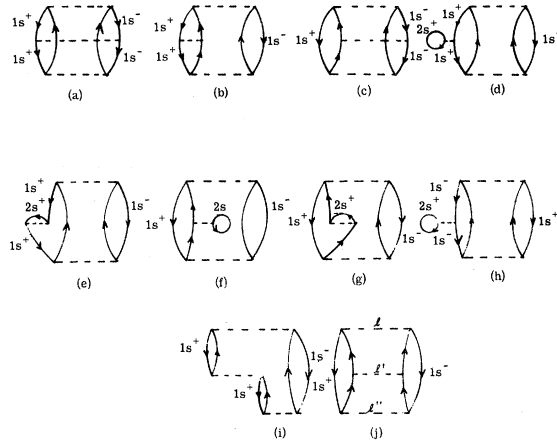[a] Includes Figs. 11(a), (b), and (c); all second-order sum to −0.419 58 a. u.

FIG. 12. Third-order energy diagrams showing various. laddering of the pair $(1s, 1s)$.

We shall next consider higher-order diagrams. As in the case of hfs, the most important higher-order diagrams are those shown in Fig. 12. The hole-hole ladders, as in (a) and (d), can be summed exactly to all orders. On the other hand, the hole-particle diagrams (b), (f), and particle-particle diagrams (m) can only be summed approximately for continuum states and exactly for the bound excited states. The bound states are, however, not very important because they contribute only 2% to the second-order energy.

The laddering of the $1s$-$2s$ correlation diagrams is not considered because the diagrams 11(e) and 11(f) are themselves rather small in magnitude as seen from Table V. Further, there is partial cancellations of diagrams, exemplified by Figs. 13(a) and 13(b), which have opposite signs since (b) has an extra internal hole line.

The process of calculation of the laddering for the $1s$-$1s$ pair in lithium can be carried out as in the case of oxygen studied by Kelly. The effects
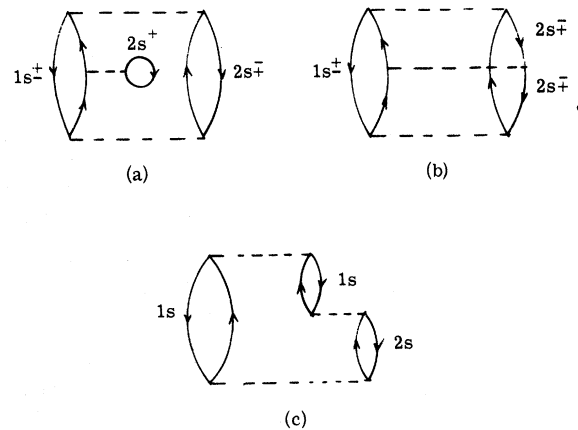

FIG. 13. Cancelling energy ladder diagrams. Diagrams (a) and (b) cancel because they are opposite in sign, since (b) has an extra internal hole line. (c) is a three-body diagram estimated to contribute negligibly to the correlation energy.

TABLE VI. Analysis of the coefficient of enhancement.

Diagram type	Values of a and t	Number of equivalent diagrams[a]	Total values of a and t
a_b	−0.105	2	−0.210
a_c	−0.105	2	−0.210
a_f	+0.042	2	+0.084
a_g	−0.001	1	−0.001
a_i	+0.011	2	+0.022
$t_{l''=l}(l'=0)$[b]	+0.105	1	+0.105
$t_{l'' \neq l}$	+0.050	1	+0.050
Total			−0.160

[a] The equivalent diagrams arise from interchanging the designations of $1s^+$ and $1s^-$ in Figs. 12(b), (c), (f), (g), and (i).

[b] Using Kelly's result for oxygen that it equals a_b.

of h-h laddering [Figs. 12(a), (d), (e), and (h)] can be carried out exactly, and can be accounted for by a shifted energy denominator[9]

$$\frac{1}{2\epsilon_{1s} - \epsilon_k - \epsilon_{k'}} \rightarrow \frac{1}{D(k,k')},$$ (37)

where $D(k,k') = 2\epsilon_{1s} - \epsilon_k - \epsilon_{k'} - \langle 1s\,1s\,|v|\,1s\,1s\rangle$

$$+ 2\langle 1s\,2s\,|v|\,1s\,2s\rangle - \langle 1s\,2s\,|v|\,2s\,1s\rangle.$$ (38)

This leads to a modified $1s$-$1s$ correlation energy of −0.037018 a.u. instead of the unmodified value of −0.039413 in Table V. The effects of h-p and p-p laddering will be handled by multiplying the modified $1s$-$1s$ diagrams by a "coefficient of enhancement"[9]

$$Ce_l(1s, 1s) = \frac{1}{1 + \sum_i a_i + \sum_i t_i}.$$ (39)

In Eq. (39), a_i is the ratio of diagrams involving one rung of the h-p ladder to the modified $1s$-$1s$ second-order diagram for a particular value of l. The suffix i refers to the particular type of ladder as exemplified by the diagrams (b), (c), (f), (g), and (i) in Fig. 12. The t_i's refer to a similar ratio for the p-p ladder, in this case Fig. 12(j). Table VI lists the contributions from these various types of ladders. Kelly[9] found Ce to be practically independent of l and we have assumed this in our calculation. On evaluating a_i and t_i for the pertinent diagrams in Fig. 12 and combining as in Eq. (31), we find the coefficient of enhancement to be 1.19 leading to the total $1s$-$1s$ correlation energy

$$E_2(1s, 1s) = -0.037018 \times 1.19 = -0.044 \text{ a.u.} \quad (40)$$

Classifying diagrams according to the bound or continuum excited states, the second-order correlation energy calculation can be separated into three types, the continuum-continuum type, continuum-bound type, and bound-bound type. In this sense, the $1s$-$1s$ intrashell calculation showed continuum-continuum contribution to be dominant (96%) while the bound-bound contribution is negligible (<0.1%). Similar behavior was found for $1s$-$2s$ intershell correlation where the continuum-type supplies over 90% and the bound-bound gives less than 1%.

As regards other higher-order diagrams, one of the important third-order diagrams is indicated in Fig. 13(c) and represents a three-particle correlation effect. Its value has been found to be 0.0002 a.u., an order of magnitude smaller than the $1s$-$2s$ correlation diagrams in 11(e) and (f). In the third-order, one can also get diagrams which represent hybrids between one-particle and two-particle interactions. Their contributions are expected to be even smaller than the diagram 13(c), since single-particle interactions in second-order [Figs. 11(a), (b), (c)] were already found to be rather small.

TABLE VII. Previous and the present calculations of the hfs and the energy of Li.

Group	Reference	Method	−E (a.u.)	hfs (a.u.)
I	15	RHF (Roothaan) variational	7.432727	2.095
	1	RHF (Goodings) numerical	7.43259	2.067
II	46	UHF	7.43275	2.825
	11	Exchange perturbation	•••	2.70
	12	Moment perturbation	•••	2.66
	48	UHFP	7.43275	2.337
	5	PUHF	7.43275	2.72
III	13	Correlated core valence	7.47631	2.883
	26	Correlated core valence	7.4778	2.826
IV	8	Configuration interaction (45 configurations)	7.47710	2.595
	27	Configuration interaction (6 configurations)	7.43185	2.872
V	28	Bethe-Goldstone equations (HF)	7.44654	2.858090
	28	Bethe-Goldstone equations (SPHF)	7.47668	2.895679
Present		Brueckner-Goldstone perturbation	7.478 ± 0.002	2.89 ± 0.02
experiment			7.47807	2.9096

Summarizing our energy results, we find that the main features of our diagrams agree with earlier work on other atoms. Thus the main part of the correlation energy (92%) arises from the second-order two-particle diagrams, Fig. 11(d), (e), and (f). Of these about 95% comes from intrashell correlation ($1s^+$-$1s^-$), and the remainder from intershell. Except for the ladder diagrams, all higher-order diagrams are effectively negligible. Among the ladder diagrams, the hole-hole and the particle-particle types are comparable and opposite in sign to the hole-particle type. The net effect of laddering is to alter the ($1s^+$-$1s^-$) correlation from -0.0394 (Table V) to -0.044 a.u. Our final correlation energy result is then -0.046 ± 0.002 a.u. as compared to $-0.045\,82$ a.u. anticipated from the experimental energy. The estimated error in our result arises mainly from the approximation procedure in calculating ladder corrections. In terms of the total energy, our calculated energy is -7.478 ± 0.002 a.u. in good agreement with the experimental value of $-7.478\,05$ a.u.

V. DISCUSSION

In order to fully appreciate the scope and merits of the BG method, we now compare our results for both the hfs and the energy with those obtained from earlier methods. Rather than discussing all the earlier results, we choose only the ones which provide the most meaningful comparisons with the present procedure. These are listed in Table VII along with our results and experiment.

The RHF results, of course, represent only the intrinsic $2s$ contribution to the hfs. We notice that both the hfs and the energy depend somewhat on the procedure for solving the Hartree-Fock equations. For comparison the intrinsic contribution from our zeroth-order wave function is 2.065 a.u., the closeness to Goodings's result being a consequence of the similarity of the procedures employed. The UHF, UHFP, and PUHF results for the hfs are best considered together. The UHF method allows for spin polarization, and naturally leads to a substantially better result than RHF. However, its close agreement with experiment may be deceptive, since as has been pointed out the UHF wave function is not an eigenfunction of S^2. This objection is removed by the PUHF procedure which restores the eigenbehavior with respect to S^2 before energy minimization. The difference of about 0.1 a.u. may be interpreted as indicative of the importance of having an eigenfunction of S^2. In our analysis, this effect is measured by the results of the (1, 1) diagrams which contribute only 0.02 a.u. Therefore we surmise that the relatively large difference of 0.1 a.u. is due to some other causes. One possibility is that the PUHF method uses a variation procedure and the result may depend sensitively on the form of the variational function. These various Hartree-Fock procedures do not explicitly include correlation, and therefore lead to essentially the same energy. Correlation effects have been explicitly included through the use of interelectronic coordinates r_{ij} and configuration interaction.

First we consider the Hylleraas-type functions. The results of two separate calculations[13],[26] with

different choices of variational functions are listed in Table VII. Both are in reasonable agreement with experiment. However, their hfs results are significantly different from each other, an effect which is symptomatic of variational calculations of this type. Berggren and Wood[13] have interpreted their hfs results to indicate that the entire difference between RHF and experiment can be explained by correlation effects alone without requiring the concept of spin polarization. Our results do not support this contention. As emphasized in Sec. III, the BG method permits a physical separation of one- and two-body effects, since these are associated with different diagrams. From Table IV, we find that about 80% of the difference between RHF and experiment arises from purely one-body diagrams which can be specifically interpreted as spin polarization effects. In fact only 15% is contributed by two-body diagrams representing correlation effects. Our conclusion about the relative importance of spin polarization effects is in agreement with the predictions of Marshall[5] and Heine.[3] Further, the validity of Heine's argument concerning the near independence of spin polarization and correlation effects is also supported by our results as indicated by the smallness of the contribution from hybrid diagrams shown in Fig. 4.

The configuration interaction results in Table VII again reflect the sensitive dependence of the hfs on the choice of variational functions. In particular, one calculation based on configurations biased towards hfs gives the expected good hfs result but a poor energy, while the reverse is true of the other calculation.[8],[27] These results have been interpreted by Nesbet[27] to indicate again the near independence of spin polarization and correlation effects.

The method using Bethe-Goldstone equations gives results in excellent agreement with experiment.[28] Analysis of the contributions to the energy reveals excellent agreement between this and the present methods. The intrashell correlation energy is $-0.041\,601$ a.u. (Nesbet) and -0.044 (ours), and the intershell correlation energy is $-0.002\,481$ (Nesbet) and $-0.002\,388$ (ours). Also, if the correlation energy is separated into contributions from excited s and non-s states, the two methods show good agreement in the individual contributions.

Three-body effects are concluded in both methods to be relatively unimportant for lithium hfs calculations. Both methods start with the RHF approximation and naturally have the same uncorrelated energy and intrinsic hfs. The contribution from spin polarization also agrees well, 0.6322 (Nesbet) and 0.675 a.u. (ours). However, there are significant differences in the other contributions to hfs. Nesbet obtains a contribution of 0.2789 a.u. to the hfs from two-particle effects, whereas we obtain 0.15. Three-particle contribution to the hfs is calculated by Nesbet to be -0.0824 a.u., which we find to be less than 0.01 and hence negligible. Further work on additional atoms should help to resolve some of these differences in detail between the two methods.

Before concluding this discussion of the relationship between the BG method and earlier ones, we would like to comment on two other perturbation

procedures, referred to as the exchange perturbation (EP) and the moment perturbation (MP) methods. These two methods are equivalent, and differ only in the order in which the exchange and the hyperfine perturbations are applied. These methods lead to contributions of 0.64 and 0.60 a.u. respectively for the spin polarization correction to hfs. These numbers compare favorably with our result 0.685 a.u. from the (0, 1) diagrams including ladders which describe the same effect.

VI. CONCLUSION

The Brueckner-Goldstone theory has been applied to the correlation energy of the lithium atom and successfully extended to the calculation of the hyperfine structure. Our results for both the hfs and the correlation energy are in very satisfactory agreement with experiment. This indicates that the BG wave function is sufficiently accurate near the nucleus as well as in the over-all volume of the atom. The one- and two-body diagrams for hfs have been separately considered to analyze their physical content. It is concluded that spin polarization accounts for the major part of the difference between RHF and experiment, while correlation effects play a smaller but significant role. Three-body effects are found to have negligible influence on the hfs as well as energy.

The present work leads us to believe that while the BG procedure would necessarily increase in complexity for heavier atoms, it would not be intractable. Since this procedure provides clear-cut answers regarding the relative importance of spin polarization and correlation effects, its extension to heavier atoms should be fruitful.

APPENDIX

Numerical Methods for Solving the Integrodifferential Equation

The equation we want to solve can be written as

$$
\left[\frac{d^2}{dr^2} - \frac{l(l+1)}{r^2} + \frac{2z}{r} + 2\epsilon - 4\left\{\frac{1}{r}\int_0^r |R_{1s^0}(r')|^2 dr' + \int_r^\infty |R_{1s^0}(r')|^2 dr'\right\}\right] R_{l,k}(r)
$$

$$
+ \frac{2}{2l+1}\left[\frac{1}{r^{l+1}}\int_0^r R_{1s^0}(r')R_{k,l}(r')r'^l dr' + r^l\left\{\int_0^\infty \frac{R_{1s^0}(r')R_{k,l}(r')}{r'^{l+1}}dr'\right.\right.
$$

$$
\left.\left. - \int_0^r \frac{R_{1s^0}(r')R_{k,l}(r')}{r'^{l+1}}dr'\right\}\right]R_{1s^0}(r) = 0, \tag{A.1}
$$

where in the exchange term, the integral $\int_r^\infty dr'$ has been rewritten as $[\int_0^\infty dr' - \int_0^r dr']$. We will solve the equation for the two cases separately: A. $\epsilon > 0$ and B. $\epsilon < 0$.

Case A. $\epsilon = k^2/2$.   The Noniterative Method

This method is based on the fact that Eq. (A.1) can be written in the form

$$
L_0 R_{l,k}(r) + f(r)\int_0^\infty R_{l,k}(r')g(r')dr' = 0, \tag{A.2}
$$

where $f(r) = 2/(2l+1)r^l R_{1s^0}(r)$ and $g(r') = R_{1s^0}(r')/r'^{l+1}$ are known functions, and L_0 is effectively just a local operator. As the name implies, the noniterative method is a means of solving Eq. (A.2) without resorting to a time-consuming iterative procedure by the following steps:

1. Solve $L_0\phi_0 = 0$. \hfill (A.3)

2. Use ϕ_0 from step 1 to solve

$$
L_0\phi_1 + f(r)\int_0^\infty \phi_0(r')g(r')dr' = 0. \tag{A.4}
$$

3. The solution of Eq. (A.2) can be shown to be a linear combination of ϕ_0 and ϕ_1:

$$
R_{l,k}(r) = \phi_0(r) + B\phi_1(r). \tag{A.5}
$$

The matching constant B can be found by substituting Eq. (A.5) into Eq. (A.2)

$$
L_0(\phi_0 + B\phi_1) + f(r)\int_0^\infty g(r')[\phi_0(r') + B\phi_1(r')]dr' = 0, \tag{A.6}
$$

which can be rewritten as

$$
L_0\phi_0 + f(r)\int_0^\infty g(r')\phi_0(r')dr' + B[L_0\phi_1 + f(r)\int_0^\infty g(r')\phi_1(r')dr'] = 0. \tag{A.7}
$$

Now using Eqs. (A.3) and (A.4),

$$
f(r)\int_0^\infty g(r')\phi_0(r')dr' + B[-f(r)\int_0^\infty \phi_0(r')g(r')dr' + f(r)\int_0^\infty g(r')\phi_1(r')dr'] = 0, \tag{A.8}
$$

$$
B = \frac{\int_0^\infty g(r')\phi_0(r')dr'}{\int_0^\infty g(r')\phi_0(r')dr' - \int_0^\infty g(r')\phi_1(r')dr'}. \tag{A.9}
$$

Now let us see why L_0 is effectively a local operator:

$$L_0 = \frac{d^2}{dr^2} - \frac{l(l+1)}{r^2} + \frac{2z}{r} + k^2 - 4\left\{\frac{1}{r}\int_0^r R_{1s0}(r')\,|^2 dr' + \int_r^\infty \frac{|R_{1s0}(r')|^2}{r'}dr'\right\}$$

$$+ \frac{2}{2l+1}\left\{\frac{1}{r^{l+1}}\int_0^r R_{1s0}(r')\phi_0(r')r'^l dr' - r^l\int_0^r \frac{R_{1s0}(r')\phi_0(r')}{r'^{l+1}}dr'\right\}\frac{R_{1s0}(r)}{\phi_0(r)}. \tag{A.10}$$

The integrals can be evaluated by Simpson's rule once the functions in the integrand are known. The exchange integrals [the last two terms of Eq. (A.10)] are then functions of $\phi_0(r_{i-2})$, $\phi_0(r_{i-1})$ and $\phi_0(r_i)$ for $L_0(r_i)$. However, the two terms in r_i cancel each other. Therefore $L_0(r_i)$ can be expressed in known functions only. The initial values for ϕ_0 can be found by assuming a power-series solution for ϕ_0 near the origin.

The equations may now be numerically integrated by Numerov's method.[17] The meshes are chosen as 0.01 from $r = 0$ to 2, and 0.05 from $r = 2$ to 50 (unit is Bohr radius a_0). The meshes in k space are picked to be 0.2 from $k = 0$ to 4, 0.5 from $k = 4$ to 10, and 1 from $k = 10$ to 20 a.u. It was only necessary to do the partial waves of $l = 0$, 1, 2, and 3.

Normalization is carried out as explained in Sec. II.D, Eq. (20), and the numerical wave functions are then stored on a magnetic tape for the computation of matrix elements.

Case B. $\epsilon < 0$. An Iterative Method due to Cooley

Cooley's original program[18] is applicable only to a local potential. One first guesses at an eigenvalue ϵ^0, e.g., from the hydrogenic energy level, and integrates inwards from a large distance until the solution reaches a maximum r_m. Then the equation is integrated outwards from the origin to r_m. The solution is matched at r_m, and from the disparity in the first derivative, a correction in eigenvalue $\Delta\epsilon$ can be calculated. With $\epsilon = \epsilon_0 + \Delta\epsilon$, this process is repeated until $\Delta\epsilon$ is less than some criteria. The only modification required is to allow for the exchange terms.

In the outward integration, the exchange is broken up into three integrals as in Case A. The integral from 0 to ∞ must be guessed and then iterated. In the inward integration, the exchange has to be regrouped.

$$\frac{1}{r^{l+1}}\int_0^r R_{1s}^0(r')R_{n,l}(r')r'^l dr' + r^l\int_r^\infty \frac{R_{1s}^0(r')R_{n,l}(r')}{r'^{l+1}}dr'$$

$$= \frac{1}{r^{l+1}}\left\{\int_0^\infty R_{1s}^0(r')R_{n,l}(r')r' - \int_r^\infty R_{1s}^0(r')R_{n,l}(r')r'^l dr'\right\}$$

$$+ r^l\int_r^\infty \frac{R_{1s}^0(r')R_{n,l}(r')dr'}{r'^{l+1}}. \tag{B.1}$$

Again the infinite integral is first guessed and then iterated.

The iterative procedure now consists of changing three numbers together: the eigenvalue and the two infinite exchange integrals. As the principal quantum number n increases, it becomes necessary to have larger and larger values of r. So there is a practical limit to how far n can go. For $n = 8$, the maximum value of r needed is 150. This value of n is more than sufficient both because higher bound states contribute so little, and because their matrix elements can easily be estimated by the $n^{-3/2}$ rule.[9] This rule is a consequence of their hydrogenic character.

$$n^{+3/2}\langle ab|v|cn\rangle = \text{constant, for all } n. \tag{B.2}$$

Summation from some bound state N_f to infinity becomes

$$\sum_{N_f}^\infty = C\int_{N_f}^\infty (n^{-3/2})^2 dn = C/[2(N_f)^2], \tag{B.3}$$

where C can be obtained from extrapolation.

A check on the program is available in the sense that the $2s$ state generated in this potential should be the same as the original $2s$ orbital taken from Roothaan, Sachs, and Weiss.

*Supported by National Science Foundation.

†Based on a thesis submitted by E. S. Chang to the faculty of the University of California, Riverside, in partial fulfillment of the requirements of the Ph.D. degree (1967). Portions of this work were reported briefly at the New York meeting of the American Physical Society; Bull. Am. Phys. Soc. **12**, 68 (1967).

‡Present address: Laboratory for Theoretical Studies, Goddard Space Flight Center, NASA, Greenbelt, Maryland.

[1] D. A. Goodings, Phys. Rev. **123**, 1706 (1961).

[2] R. E. Watson and A. J. Freeman, Phys. Rev. **123**, 2027 (1961); N. Bessis, H. Lefebvre-Brion, C. M. Moser, A. J. Freeman, R.K. Nesbet, and R. E. Watson, Phys. Rev. **135**, A588 (1964).

[3] V. Heine, Czech. J. Phys. **B13**, 619 (1963).

[4] C. M. Sachs, Phys. Rev. **117**, 1504 (1960).

[5] W. Marshall, Proc. Phys. Soc. (London) **A78**, 113 (1961); J. Phys. Soc. Japan **17**, Suppl. B-I, 20 (1962).

[6] E. A. Hylleraas, Z. Physik **54**, 347 (1929).

[7] H. M. James and A. S. Coolidge, Phys. Rev. **49**, 688 (1936); **55**, 873 (1939).

[8] A. W. Weiss, Phys. Rev. **122**, 1826 (1961).

[9] H. P. Kelly, Phys. Rev. **131**, 684 (1963); **136**, B896 (1964); **144**, 39 (1966).

[10] R. T. Pu and E. S. Chang, Phys. Rev. **151**, 31 (1966).

[11] M. H. Cohen, D. A. Goodings, and V. Heine, Proc. Phys. Soc. (London) **73**, 811 (1959).

[12] G. D. Gaspari, W. M. Shyu, and T. P. Das, Phys. Rev. **134**, A852 (1964).

[13] K. F. Berggren and R. F. Wood, Phys. Rev. **130**, 198 (1963).

[14] J. Goldstone, Proc. Roy. Soc. (London) **A239**, 267 (1957).

[15] C. C. J. Roothaan, L. M. Sachs, and A. W. Weiss, Rev. Mod. Phys. **32**, 186 (1960); E. Clementi, IBM J. Res. Develop. **9**, 2 (1965).

[16] R. Marriott, Proc. Phys. Soc. (London) **72**, 121 (1958).

[17] M. G. Salvadori and M. L. Baron, Numerical Methods in Engineering (Prentice-Hall, Inc., Englewood Cliffs, N. J., 1961).

[18] C. W. Cooley, Math. Computations **15**, 363 (1961).

[19] E. Fermi, Z. Physik **60**, 320 (1930).

[20] N. F. Ramsey, Nuclear Moments (John Wiley & Sons, Inc., New York; Chapman & Hall, Ltd., London, 1953).

[21] R. H. Lambert and F. M. Pipkin, Phys. Rev. **128**, 198 (1962).

[22] N. F. Ramsey, Molecular Beams (Oxford University Press, 1956).

[23] R. K. Nesbet, Quantum Theory of Atoms, Molecules, Solid States (Academic Press, Inc., New York, 1966).

[24] C. L. Pekeris, Phys. Rev. **112**, 1649 (1958); **115**, 1216 (1959).

[25] C. W. Scherr, N. J. Silverman, and F. A. Matsen, Phys. Rev. **127**, 830 (1962), see Tables V and VI.

[26] E. A. Burke, Phys. Rev. **135**, A621 (1964).

[27] R. K. Nesbet, Phys. Rev. **118**, 681 (1960).

[28] R. K. Nesbet, in Proceedings of the International Colloquium No. 164 on the Magnetic Hyperfine Structure of Atoms and Molecules, Paris, 1966 (Centre National de la Recherche Scientifique, 1967), p. 87; for other energy calculations with Bethe-Goldstone method, see R. K. Nesbet, Phys. Rev. **155**, 56 (1967).

Many-Body Calculation of Atomic Polarizability –Relation to Hartree-Fock Theory*

Edward S. Chang,† Robert T. Pu, and T. P. Das
Department of Physics, University of California, Riverside, California
(Received 6 November 1967)

The Brueckner-Goldstone perturbation method has been applied to the calculation of the dipole polarizability (α_d) and antishielding factor (γ_d) for lithium-atom ground state. The complete set of states utilized is the same as those employed in earlier calculations of the hyperfine constant and correlation energy. Our results are $\alpha_d = 24.84$ Å^3 and $\gamma_d = 0.958$, as compared to a recent experimental value for $\alpha_d = 22 \pm 2$ Å^3 and $\gamma_d = 1.000$ from the Hellmann-Feynman theorem. The relationship between the Brueckner-Goldstone and the Hartree-Fock perturbation procedures is discussed with reference to specific physical effects.

I. INTRODUCTION

In an earlier paper,[1] referred to as I, we have applied the Brueckner-Goldstone[2] (BG) formalism to the study of the hyperfine constant and the energy of lithium as a test of the atomic ground-state wave function. In the present work, we shall investigate the atomic dipole polarizability (α_d) and the induced electric field at the nucleus which is characterized by the shielding factor (γ_d), both of which have been studied earlier for beryllium and oxygen atoms by Kelly.[3,4] These properties require the ground-state wave function as well as the perturbed wave function in an external field, and therefore provide additional test of the unperturbed wave function. Our aim in the present work is twofold; first, to utilize the diagrammatic technique to study the relative importance of various physical effects that contribute to the polarizability, similar to our earlier analysis of the hyperfine in-